Experimental demonstration of a slippage-dominant free-electron laser amplifier

X. Yang, Y. Shen, B. Podobedov, Y. Hidaka, S. Seletskiy, and X. J. Wang

Experimental demonstration of a slippage-dominant free-electron laser amplifier

X. Yang, Y. Shen, B. Podobedov, Y. Hidaka, S. Seletskiy, and X. J. Wang

National Synchrotron Light Source, Brookhaven National Laboratory, Upton, NY 11973

We report the first experimental demonstration of a slippage-dominant free-electron laser (FEL) amplifier using a 140 fs (FWHM) broadband seed-laser pulse. The evolution of the longitudinal phase space of a laser seeded FEL amplifier in the slippage-dominant regime was experimentally characterized. We observed, for the first time, that the pulse duration of the FEL is primarily determined by the slippage between the seed laser and the electron beam. With a ±1% variation in the electron beam energy, we demonstrated reasonably good longitudinal coherence and ±2% spectral tuning range. The experimentally observed temporal and spectral evolution of the slippage-dominant FEL was verified by the numerical simulations.

I. INTRODUCTION

With the recent successful commissioning of the Linac Coherent Light Source (LCLS) at SLAC National Accelerator Laboratory [1], free-electron lasers (FELs) offer great promise of becoming the premier source of tunable, intense, coherent photons for either ultra-short time resolution (single pass amplifier) or ultra-fine spectral resolution (oscillator), over a wide range of wavelengths from THz to the hard X-ray regime. Among several major approaches for single-pass FELs, Self-Amplified Spontaneous Emission (SASE) FELs have excellent tunability and transverse coherence but poor temporal coherence since the lasing process starts from the shot noise of the electron beam [2,3]. Laser-seeded FEL amplifiers have good temporal coherence since an external coherent seed laser pulse initiates the FEL process [4,5,6]. However, the external seed determines the wavelength of the output radiation [5]. Therefore, the tunability of such an FEL depends upon the seed.

In this report, we experimentally investigate a novel spectro-temporal regime of a laser-seeded FEL amplifier, whose pulse length is primarily determined by the slippage between the seed laser and the electron beam. The wavelength of the FEL radiation is centered at the spontaneous radiation wavelength,

$$\lambda_r = \frac{\lambda_U}{2\gamma_r^2}(1 + \frac{K^2}{2}) \qquad (1)$$

determined by the electron beam energy $mc^2\gamma_r$. $K = eB_u/mck_u$ is the dimensionless undulator parameter and λ_u, k_u, and B_u are the undulator wavelength, wave number, and magnetic field respectively [7]. We provide theoretical and experimental evidence for the spectral overlap between the seed laser pulse and the FEL gain bandwidth (GBW), which initiates the FEL process. The FEL output preserves the tunability of SASE while maintaining the longitudinal coherence of the seed laser. This dynamical behavior, which we have dubbed "slippage-dominant FEL amplification", occurs in seeded FELs with short seed pulse duration and large slippage $L_s = N_r \cdot \lambda_r$, where slippage is defined as the displacement of the optical pulse with respect to the electron beam at the end of the N_r periods of the undulator. Such amplification may be relevant for the next generation of tunable high-power seeded FELs. However, the ultimate limit on the spectral tuning range is set by the seed laser bandwidth. The tunable short-wavelength limit λ_{sl} and FEL power amplification are set by the slippage.

In a slippage-dominant FEL amplifier, the bandwidth of the seed laser ($\geq 10^{-2}$) is significantly larger than the GBW of the FEL, which is on the order of the FEL Pierce parameter $\rho \sim 10^{-3}$ [3,8]. This situation is similar to frequency pulling in conventional lasers when the bandwidth of the gain medium is much larger than the bandwidth of the laser cavity and the frequency of the laser output is mainly determined by the frequency of the cavity mode [9]. In the FEL case, the lasing frequency is dominated by the resonant frequency of the FEL (λ_r) instead of the frequency of the seed laser (λ_{SEED}). When the FEL electron beam energy is detuned such that $\lambda_r \neq \lambda_{SEED}$, the spectral overlap between the seed laser and the FEL GBW provides the initial seed to bunch the electrons in the slippage region before they start to emit coherent light, in an identical way to the generation of the superradiant spike in the slippage regime [10], called SSPIKE. The pulse length of SSPIKE prior to saturation is proportional to the slippage length, $\sim 0.5L_s$. The FEL power amplification and the short wavelength limit λ_{sl} at which the FEL gain process becomes less efficient, i.e., when its intensity is less than that of the seed pulse, are determined by the magnitude of the slippage.

A superradiant FEL amplifier has been experimentally characterized previously [11]. Here we report the experimental demonstration of a slippage-dominant FEL amplifier, similar to a

superradiant FEL except in the linear regime, using a short seed-laser pulse (140 fs FWHM) at a fixed central wavelength (793.5 nm) and a variable energy electron beam (100.7 – 102.8 MeV). The pulse length of the observed SSPIKE is determined by the slippage. Simultaneously, we observed the FEL output as a single spike centered at the resonant wavelength, which indicates good longitudinal coherence. Our measurements demonstrate a significant (±2%) spectral tuning range, 778 nm to 810 nm when a 140 fs seed laser pulse with 1% bandwidth (FWHM) is used. The tunable range of the FEL is defined by the range of wavelengths for which the FEL energy output exceeds by the minimum of tenfold that of the SASE FEL. In addition, the FEL output power is up to three orders of magnitude higher than that generated by the SASE FEL. Our experimental findings agree reasonably well with the results of our simulations using the PERSEO code [12].

II. SIMULATION

PERSEO code was used to simulate our short-pulse seeding experiment. It allows 1D simulation of single pass FEL amplifiers and oscillators. Also, it includes higher order harmonics and handles startup from either shot-noise or an external coherent laser source. Time dependent simulations have been programmed within Mathcad. The core routine solves the pendulum-like FEL equations coupled with the field equations which govern the FEL longitudinal dynamics [13,14].

We begin with a PERSEO simulation under the realistic short-pulse experimental condition where the seed-laser pulse length is on the order of the cooperation length L_c, which is given by the slippage in one gain length ($\lambda_r/4\pi\rho$). We use a Gaussian temporal profile model for the electron bunch, cut off at six standard deviations from the center and the same time window for the seed laser pulse. In the simulation, three distinct FEL processes always coexist: SASE, direct amplification of the seed (ASEED), and SSPIKE. ASEED, identical to the laser-seeded FEL in the steady-state regime, describes the seed-laser pulse itself temporally evolving through the undulator. SSPIKE is the FEL radiation from the electrons in the slippage region. Their radiation output can be qualitatively described as

$$P_{out}(Z) \approx P_{ini} \cdot \int_0^L e^{\Gamma(\delta,s)\cdot Z} ds \qquad (2)$$

where $\Gamma(\delta,s)$, L, P_{ini}, and P_{out}, are the growth rate, interaction length, initial seed power, and output radiation power of an FEL, respectively. Longitudinal coordinates Z along the undulator and s along the electron bunch are defined within $0<Z<L_u$ and $0<s<L_e$ respectively, where L_u and L_e

are the undulator length and the electron bunch length. The detuning parameter, $\delta = (E-E_s)/(\rho E_s) = \delta_e/\rho$, describes the deviation of the electron beam energy E relative to the seed resonance energy $E_s=mc^2\gamma_s$. Here,

$$\gamma_s = \sqrt{\frac{\lambda_u}{2\lambda_{SEED}} \cdot \left(1+\frac{K^2}{2}\right)}. \qquad (3)$$

In the SASE case, the FEL process starts from the shot noise of the electron beam P_{SNoise}. SASE is always on-resonance ($\delta=0$) and occurs throughout the entire electron bunch ($L= L_e$), yielding excellent tunability but rather poor longitudinal coherence. In the ASEED case, L is equal to the seed pulse length L_{SEED}, P_{ini} is equal to the seed power P_{SEED}, and the growth rate $\Gamma(\delta,s)$ falls sharply when δ is large. ASEED has no spectral tunability [5]. In the SSPIKE case, the growth rate is at the maximum value $\Gamma(0,s)$, L is equal to the slippage L_s, and $P_{ini}=P_{SSPIKE}$ is the fraction of the seed power that falls within the FEL GBW. Depending on P_{SEED}, P_{SSPIKE} could far exceed P_{SNoise} once the electron beam energy detuning is well within the seed bandwidth. Furthermore, linear analysis predicts that ASEED is negligible even when the detuning parameter $\delta = 0$ [15], as long as the slippage length L_s ($\geq 10L_c$ normally) is significantly greater than the seed pulse length, i.e. in the short pulse condition. SSPIKE becomes dominant among these three FEL processes.

To realize a coherent tunable FEL source through SSPIKE, we are interested in the large detuning case. In the high-gain steady-state limit, when $\delta > 3/2^{2/3} \approx 1.89$, the steady-state interaction terminates and the seed pulse is effectively unperturbed when it slips through the electron bunch along the undulator, except that a portion of the seed spectrum overlapping the FEL GBW provides the initial seed to coherently bunch the electrons in the slippage region. The key experimental parameters used in the simulation are listed in Table I.

TABLE I. Experimental parameters at the SDL

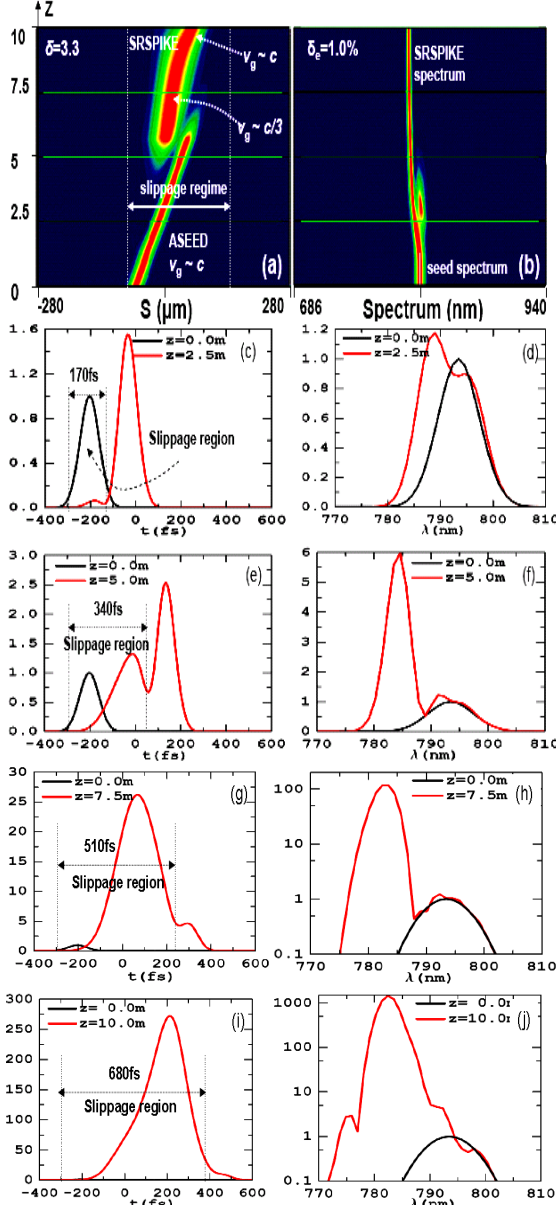|	
Undulator period λ_u	3.89 cm
Undulator parameter K	1.1
Undulator length L_u	10 m
Electron beam energy detuning δ_e	1%
Electron bunch length (FWHM)	1.1 ps
rms energy spread $\Delta E/E$	0.1%
Maximum peak current I	350 A
Seed laser wavelength λ_{SEED}	793.5 nm
Seed laser bandwidth (FWHM) $\Delta\lambda_{SEED}$	7.5 nm
Seed laser duration (FWHM) τ_{SEED}	140 fs
Peak power of seed laser	1 MW

FIG. 1 (color). (a) Normalized longitudinal profile of the radiation power along the electron beam coordinate s as it evolves along the undulator with coordinate z, and (b) spectral evolution along the undulator, as determined by a numerical simulation with PERSEO using the experimental parameters given in the Table 1 and δ=3.3. (c-j): input seed pulse (black curves) and FEL output (red curves). Temporal (c, e, g, i) and spectral (d, f, h, j) profiles (–) along the undulator coordinate z, scaled relative to the intensity of the initial seed. (c) and (d) at z=2.5m, (e) and (f) at z=5.0m, (g) and (h) at z=7.5m, and (i) and (j) at z=10m.

In our simulation, only one spike is observed in the temporal and spectral evolution along the undulator, as shown in Figs. 1(a) and 1(b) respectively. In Fig. 1(a), we observe the spike evolving through the exponential gain regime ($v_g \sim c/3$) before arriving at the superradiant regime ($v_g \sim c$) at the end of the undulator, where v_g is the group velocity of FEL radiation pulse. In the FEL process, starting from the lethargy region at z = ~2.5m, through the exponential gain region ~5.0 m < z < ~9.0 m, a majority of the seed spectrum stays the same, except that the part overlapping with the FEL GBW participates in the FEL interaction by providing the initial seed to coherently bunch the electrons in the slippage region, shown by red curves in Figs. 1(d), 1(f), and 1(h) (black curves represent the initial seed). Because the detuning parameter, δ=3.3, is large, the seed pulse maintains its temporal shape, shown as the part of the red curves immediately in front of the slippage region in Figs. 1(c), 1(e), and 1(g). In the temporal domain, a single SSPIKE in the slippage region starts to grow, as shown in Figs. 1(c) and 1(e), until it dominates over the seed, as shown in Fig. 1(g). The energy gain of the SSPIKE relative to the seed laser is ~100 at the end of exponential gain region. The temporal and spectral profiles become distorted when the FEL process evolves into the saturation region, as shown in Figs. 1(i) and 1(j). Besides reproducing superradiant spiking phenomena in the linear regime, we observe a single spike spectral behavior with a SSPIKE pulse width of ~$0.5 L_s$ (FWHM) before the saturation.

III. EXPERIMENT

We conducted the experiments described here at the Source Development Laboratory (SDL) of the National Synchrotron Light Source (NSLS), Brookhaven National Laboratory. The SDL is a laser linac facility featuring a high-brightness electron source, a 4-magnet chicane bunch compressor, an S-band SLAC type traveling-wave linac, and a Ti:sapphire laser system [16]. The 100 MeV high-brightness electron beam passes through the NISUS undulator [17], a 10-m-long planar undulator consisting of 16 sections, with a period of 3.89 cm. The Ti:sapphire seed laser, which is also the photo-cathode drive laser, is based on chirped pulse amplification (CPA). After splitting the amplified laser pulse into two parts, they pass through two independent optical grating compressors. One compressed laser pulse is frequency-tripled to the UV wavelength for the photo-cathode RF gun. The other one is compressed down to a Fourier-transform-limited width of 140 fs for seeding the FEL amplifier. Using a single laser for generating both the electron beam and the amplifier seed minimizes the timing jitter. The principal parameters in the experiment are the same as those used in the simulations described earlier.

We measured FEL output spectra in the range of beam energy from 100.7 (δ = -3.03) to 102.8 MeV (δ = +3.03) using a single-shot Ocean Optics

spectrometer with 0.3 nm resolution. The electron beam energy jitter in any given run is about 0.5% (peak-to-peak). By adjusting the electron beam energy above and below the seed-laser resonance, we observed significant changes in the FEL spectra, as illustrated in Fig. 2.

Spectra corresponding to three different electron beam energy detuning values, $\delta_e = 0.91\%$, 0.0%, and -0.91%, are shown in Fig. 2. Their corresponding spectral peaks, located at 779 nm, 793 nm, and 808 nm, are scaled according to the measured FEL output energy. There is good agreement between the experimental and simulated spectra, especially in peak locations and spectral widths, demonstrating that the electron beam energy determines the spectrum.
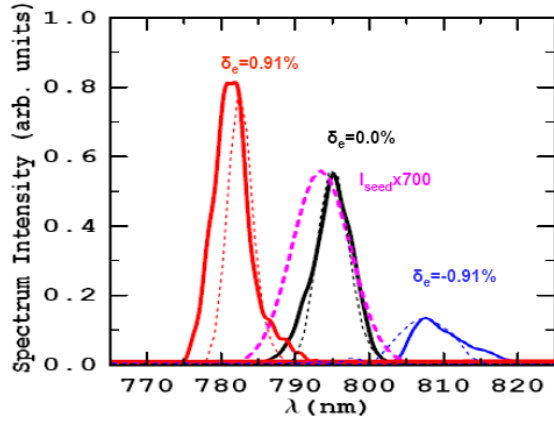

FIG. 2 (color). Experimental and simulated spectra at three electron beam energy detuning values: +0.91% (—) and (---), on-resonance (—) and (---), and -0.91% (—) and (---). Seed spectrum multiplied by 700 (--). Seed energy 0.1 µJ. SASE output ~0.03 µJ, constant in the detuning range (not shown).

FIG. 3 (color). Variation of FEL output with beam energy: experiment (--), simulation (—), and simulation in the long pulse case (-o-). (a) normalized energy output, and (b) deviation of FEL output peak spectrum with respect to to the seed laser [5]. The maximum FEL output in (a) is 120 µJ.

The FEL radiation was directed to a diagnostic station where pulse energy was measured with a calibrated joulemeter. The timing jitter between the seed laser and the electron beam, mainly caused by shot-to-shot variations in the RF phase and amplitude which lead to changes in the beam energy and peak current, engenders shot-to-shot fluctuations in the FEL output, as reflected in the magnitude of the root-mean-square (rms) error bars in Fig. 3.
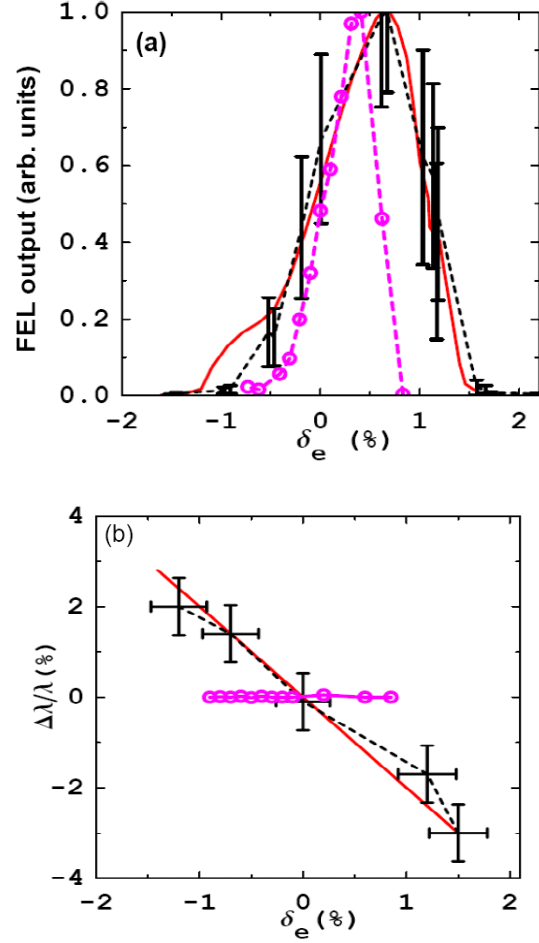
Comparisons between the experimental findings and the PERSEO simulations of the output pulse energy and the deviation of FEL peak spectrum versus the electron beam energy detuning δ_e are shown in Figs. 3(a) and 3(b), respectively, where we represent the experimental data with a black dashed line with rms error bars. Evidently, the output energy initially increases with the detuning of the beam energy above resonance. Both the experiment and the simulation show that the largest enhancement occurs when the beam energy increases by about 0.65% from the resonant energy. A decrease in beam energy by a similar amount significantly reduces the FEL efficiency [5]. The wavelength of the FEL output radiation is centered at the spontaneous undulator radiation wavelength. The deviation of the FEL spectral peak satisfies the relationship $(\lambda - \lambda_{SEED})/\lambda_{SEED} \approx -2 \cdot \delta_e$ as a function of electron beam energy detuning δ_e.

It has demonstrated previously, in both experiment and simulation, that the FEL gains with detuning are asymmetric between positive and negative detuning values; positive detuning enhances the gain by about a factor of two, while negative detuning degrades it by a similar amount [5]. This has been explained using 1D steady-state theory [18,19]. In the early stage of amplification, small-signal gain theory indicates that the direction of energy deposition between electrons and radiation is opposite, depending on the direction of detuning. The radiation energy in the negative detuning case is deposited to electrons, while that with positive detuning immediately gains energy from electrons. On resonance, there is no energy deposition. In the high gain regime, a cubic equation for time-dependent gain of FEL radiation in the form $e^{i\lambda\tau}$ is written as $\lambda^3 - \delta \cdot \lambda + 1 = 0$, where λ is an eigenvalue, of which the negative imaginary part gives the growth rate. The Pierce parameter is assumed to be small, $\rho \sim 0$. The instability exists only when the detuning is smaller than the threshold, i.e., $\delta < \delta_{th} \sim 1.89$, where two of the three eigenvalues have an imaginary part. Ultimately, this can be explained as the radiation power build up from electrons trapped and rotating in the phase space bucket. It is expected that the power growth will stop when majority of the electrons are accumulated at the low energy end of the phase space bucket. Due to energy conservation, the FEL gain, which is equal to the total energy loss of electrons, is optimized at the maximum positive detuning, $\delta_{th} \sim 1.89$, beyond which the FEL interaction is terminated. It also has been numerically shown that as the electron energy increases, the saturation energy becomes higher until it reaches the threshold, $\delta \sim \delta_{th}$. Since the Pierce parameter ρ is ~0.003, the threshold corresponds to an electron energy detuning value of 0.6%, which is consistent with the measured and simulated value in this work of $\delta_e = 0.65\%$ shown in Fig. 3(a).

It is instructive to compare the short-pulse regime to the well-known long-pulse or steady-state regime. The simulated long-pulse case with a 10 ps (FWHM) seed pulse duration is shown by the magenta curve in Figs. 3(a) and 3(b). The electron beam energy detuning range in the short pulse case is about -1% to 1.5%, which is approximately a factor of two greater than in the long pulse case (-0.5% to 0.7%). There is no tunability of the FEL spectrum in the long pulse case since the seed laser has narrow bandwidth and only the steady-state region exists in the FEL process [5].
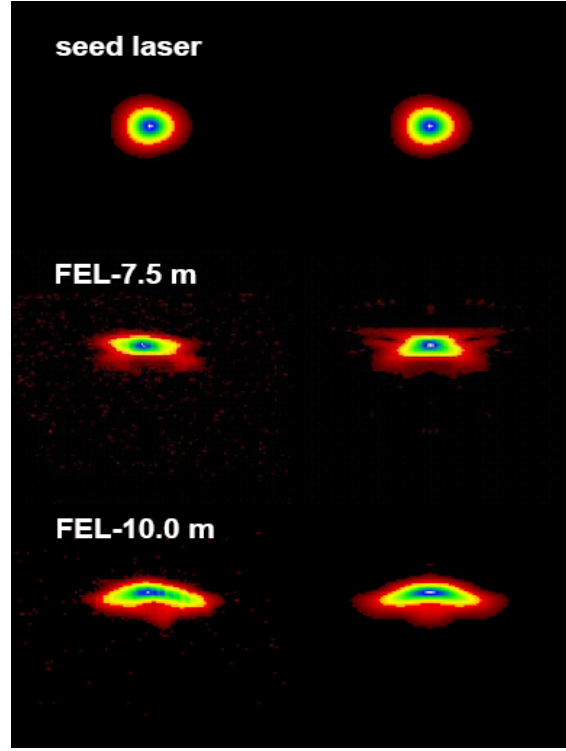
(a)
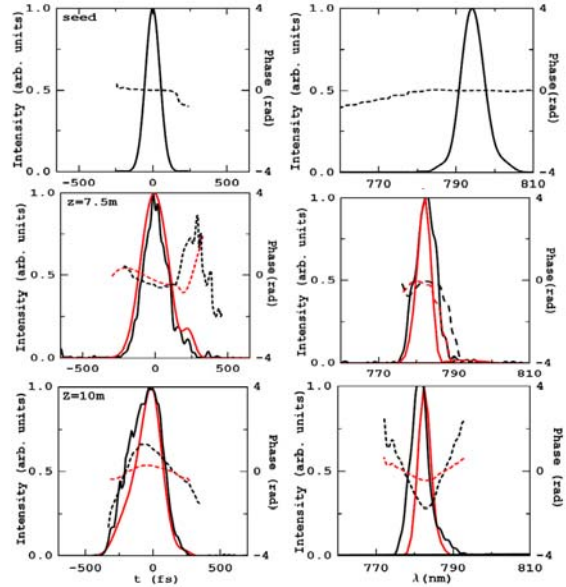
(b)

FIG. 4 (color). (a) Measured (left column) and retrieved (right column) FROG traces. (b) Retrieved (black) and simulated (red) intensity (solid) and phase (dash) in temporal and spectral domains. Seed energy is 0.1μJ.

The longitudinal phase space distribution of the radiation is measured using a commercial Grenouille configuration FROG [20]. At the electron beam energy detuning value $\delta_e = 0.91\%$, similar to the ones used in the simulation of Fig. 1, the raw and retrieved FROG images of the FEL

light are shown in the left and right columns of Fig. 4(a) respectively, where the horizontal axis is the delay [τ] and the vertical axis is the frequency [ω], along with a label which highlights the longitudinal position in the undulator where the FEL interaction was terminated while we were taking the FROG data. The FROG image of the input seed laser is shown in the top row of Fig. 4(a). The resulting temporal and spectral distributions (solid lines) and phase (dashed lines) are shown in left and right columns of Fig. 4(b). The FEL interaction was terminated by using a trim coil located at various points along the undulator to kick the beam off the ideal trajectory. The FROG measurements (─) and simulated (─) temporal and spectral distributions agree reasonably well. At z = 7.5 m and 10 m in the undulator, the FROG measurements indicate that the linear phase variation in the temporal domain is dominant and results in a frequency shift, which is given by $\omega(t) = - d\varphi(t) / dt$, leading to a blueshift. Based on our time-dependent PERSEO simulation results, this is due to the positive energy detuning. The linear phase variations are removed from both the measurements and simulations in order to show the smaller nonlinear phase. Both the measurements and simulations indicate that there is a positive chirp in the time domain at z = 10 m, which is consistent with the FEL intrinsic chirp [21,22]. However, the simulated chirp is significantly smaller compared to the measured one.

Since the slippage regime is dominant when δ_e = ±0.91%, we experimentally confirm that a single SSPIKE grows out of the slippage regime, as shown in the right column of Figs. 4(a) when z = 7.5 m and z = 10.0 m and it dominates over the seed when z ≥ 7.5m. At z = 10 m, the pulse duration of the SSPIKE measured using the FROG is ~330 fs (FWHM) which is much wider than the seed-laser pulse (140 fs FWHM) and is about half of the slippage length (680 fs). In the temporal domain, these electrons slipped over by the seed-laser pulse are coherently bunched before they start to emit coherent FEL light. Therefore, the time-bandwidth products Δτ·Δν reconstructed from these FROG images are well within a factor of two of being Fourier transform limited, implying that the FEL pulse has reasonably good longitudinal coherence.

IV. CONCLUSION

In conclusion, we report the experimental demonstration of the slippage-dominant FEL amplifier using an ultrafast seed-laser pulse. For a FEL amplifier operating in this regime, we experimentally and numerically characterize the evolution of its longitudinal phase space along the undulator, and show that the FEL spectrum is tunable while its temporal distribution is determined by the slippage. We also provide numerical and experimental evidence for the spectral overlap between the seed pulse and the FEL GBW, which initiates the slippage-dominant FEL process, rather than a process starting from the shot noise of the electron beam. For the 140 fs seed laser pulse at a fixed central wavelength of 793.5 nm and ~1.1 ps electron bunch duration, ±2% spectral tunability was experimentally demonstrated. Furthermore, we observe a radiation pulse with reasonably good longitudinal coherence at δ_e = ±0.91% using a FROG. Both simulations and experiments reveal greatly improved longitudinal coherence of the FEL output compared to that of SASE. Also, the FEL output power is up to three orders of magnitude greater than that generated by a SASE FEL. These results agree well with our numerical simulations. More detailed studies of the phase information can lead to a better understanding of this scheme, its capabilities, and ultimate performance. How to apply this scheme as a broad-band tuning technique and further extend it towards shorter wavelengths will be the subject of our future work.

IIV. Acknowledgments

[1] P. Emma for the LCLS team, Nature Photonics 4, 641 (2010).

[2] A. Kondratenko *et al*., Part. Accel. **10**, 207 (1980).

[3] R. Bonifacio *et al*., Opt. Commun. **50**, 373 (1984).

[4] L.H. Yu *et al*., Science, **289**, 932 (2000).

[5] X.J. Wang *et al*., Appl. Phys. Lett. **91**, 181115 (2007).

[6] G. Lambert *et al*., Nature Physics **4**, 296 (2008).

[7] W. B. Colson, IEEE J. Quantum Electron. **17**, 1417 (1981).

[8] W.A. Barletta *et al*., Nucl. Instrum. and Method Phys. Res. Sect. A **618**, 69 (2010).

[9] A. Yaryv, Quantum Electronics, John Wiley & Sons Inc., NY, 1989.

[10] R. Bonifacio *et al*., Phys. Rev. A **44**, R3441 (1991).

[11] T. Watanabe *et al*., Phys. Rev. Lett. **98**, 034802 (2007).

[12] L. Giannessi, Proc. of FEL 2006, BESSY, Berlin, Germany, 91 (2006).

[13] W. B. Colson, Laser Handbook vol **6**, 301 North-Holland, Amsterdam, 1990.

[14] W. B. Colson *et al*., Phys. Rev. A **31**, 828 (1985).

[15] S.Y. Cai *et al*., Phys. Rev. A **42**, 4120 (1990).

[16] J.B. Murphy *et al*., Synchrotron Radiation News (SRN) Vol 21, No. 1, 41 (2008).

[17] D.C. Quimby *et al*., Nucl. Instrum. and Method Phys. Res. Sect. A 285, 281 (1989).

[18] J.B. Murphy *et al*., Nucl. Instrum. and Method Phys. Res. Sect. A **237**, 159 (1985).

[19] T. Watanabe *et al*., Proc. of FEL 2006, MOPPH065 (2006).

[20] D.J. Kane and R. Trebino, IEEE J. Quantum Electron. 29, 571 (1993).

[21] Y. Li *et al*., Phys. Rev. Lett. **89**, 234801 (2002).

[22] S. Krinsky *et al*., Phys. Rev. ST. Accel. **6**, 050702 (2003).